


L. CHEN
X.Y. ZHOU
G.P. WANG*,

V-shaped metal–dielectric multilayers for far-field subdiffraction imaging

Key Laboratory of Acoustic and Photonic Materials and Devices, Ministry of Education and Department of Physics, Wuhan University, Wuhan 430072, P.R. China

Received: 2 March 2008/Revised version: 8 May 2008
Published online: 20 June 2008 • © Springer-Verlag 2008

ABSTRACT We propose a kind of v-shaped planar silver and dielectric multilayers for far-field subdiffraction imaging. Finite difference time domain simulations reveal that two linear sources with a separation far below the diffraction limit can be magnified by the systems to the extent that conventional far-field optical microscopy can be further manipulated.

PACS 78.67.Pt; 07.60.Pb; 42.79.-e; 78.20.-e

1 Introduction

The diffraction limit of light, which is caused by the loss of evanescent waves that carry high spatial frequency information, limits the resolution of conventional lenses to the order of the wavelength of light used to image the object. Near-field scanning optical microscopy can overcome this limit [1] to reach a much finer resolution beyond the diffraction limit and has led to the possibility of resolving details on the order of the 10–100 nm scale [2]. But the major constraint of this invention may be the need for scanning the sample point by point, making the entire procedure relatively slow and thus, in principle, preventing it from capturing the fast dynamic process taking place in the sample in real time. The recently proposed “superlens” offers that possibility, but the amplified image can not be processed by conventional optics because the image is still in the near field [3–5]. It is highly desirable for many applications to use a system which would produce a direct optical far-field

image that carries subwavelength features. Quite recently, theoretical and experimental studies demonstrated a kind of hyperlens, which is constructed with layered media with a hyperbolic dispersion and can carry evanescent waves to the far field along the normal direction of the layered medium [6–10]. However, the reported hyperlenses so far utilize cylindrical geometry, which is not easy to perfectly realize in common cases and hence technologic aberration in the fabricating process may destroy the resultant resolution of the systems. Although a planar layered structure with inclined output plane was also proposed for the far-field superresolution imaging [7], the optical paths from different objects to the imaging plane are different, which will result in the variation of image intensity and hence may lead to misreading to the images.

Since Economou’s pioneering work on periodic structures consisting of nanoscale metal and dielectric layers [11], subwavelength metal–dielectric multilayers were revealed to show very attractive properties [12–18]. Most re-

cently, it was suggested that such layered metal–dielectric media show the capability of almost undistortedly transferring an optical field distribution in a plane to any other arbitrary plane through the rays parallel to the axis of the layered structure, as if the dielectric functions of metal (ϵ_m) and dielectric (ϵ_d) satisfy the relation of $\epsilon_m + \epsilon_d \rightarrow 0$ [19–21]. This is essentially because of the anisotropic property of light propagation in the layered materials, which can support propagation waves with very large wavenumbers in some designed directions. Based upon the principle, instead of using the nonplanar structures, we will introduce a planar silver and dielectric multilayered v-shaped hyperlens (VSHL) for far-field subdiffraction imaging. The feasibility of the VSHL for the far-field superresolution imaging will be demonstrated by using two-dimensional finite difference time domain (FDTD) simulations. It should be pointed out that, similar to all the previous reports such as [8, 10], the hyperlens demonstrated here is also just suitable for magnifying linear objects oriented in a proper direction.

2 VSHL structure and imaging properties

Figure 1 illustrates the suggested VSHL constructed by alternatively stacking two-dimensional planar Ag films and dielectric films. Where d_1 , d_2 and ϵ_m , ϵ_d are the thickness and dielectric constant of Ag films and dielectric films, respectively. θ and d denote the wedge angle and total thickness of the VSHL, respectively. The blue dotted lines 1 and 2 represent the input and out-

* Fax: +86-27-68764131, E-mail: kp_wang@hotmail.com

* Present address: Key Laboratory of Acoustic and Photonic Materials and Devices, Ministry of Education and Department of Physics, Wuhan University, Wuhan 430072, P.R.China

put surfaces of the VSHL, respectively. In our FDTD simulations, the spatial and temporal steps are set at $\Delta x = \Delta y = 5$ nm and $\Delta t = \Delta x/2c$ (c is the velocity of light in vacuum), and the perfectly matched layer absorbing boundary condition is used at the boundaries of the computational window [22]. The exciting light is a TM-polarized wave (magnetic field parallel to the z -direction) with wavelength $\lambda = 365$ nm, and the relative dielectric constants of the Ag and dielectric films are $\varepsilon_m = -2.4012 + j0.2488$ and $\varepsilon_d = 2.4$, respectively [23].

To know the far-field imaging characteristics of the VSHL, we first consider two linear sources A and B separated by $d_{AB} = \lambda/3$ and symmetrically placed on the input surface of a VSHL made of 36 pairs of alternating Ag and dielectric layers with $d_1 = d_2 = 10$ nm and $d = 720$ nm $\simeq 2\lambda$. Figure 2a–c show the amplitude distributions of the magnetic field $|H_z|$ in the region bounded by the rectangle denoted in Fig. 1, as θ is set at 45, 90, and 135°, respectively. From the figures, one can see that the radiating lights from the two linear sources travel along the normal directions of the system and then enter into the air at the output boundary surface of the VSHL to form two images A' and B'.

Figure 3 shows the $|H_z|^2$ profile distributions of two linear sources along the input surface (Fig. 3a) and their output images on the output surface (Fig. 3b) of the VSHL, respectively, in the case of $\theta = 90^\circ$ (Fig. 2b). From the figures, we can see that the curve distance ($d_{AO} + d_{OB}$) of two linear sources on the input surface is amplified from 0.47λ to 4.5λ on the output surface ($d_{A'O'} + d_{O'B'}$), corresponding to the straight distances of the two linear sources from $d_{AB} = 0.47\lambda/\sqrt{2} \simeq \lambda/3$ to $d_{A'B'} = 4.5\lambda/\sqrt{2} \simeq 3.2\lambda$ of the out-

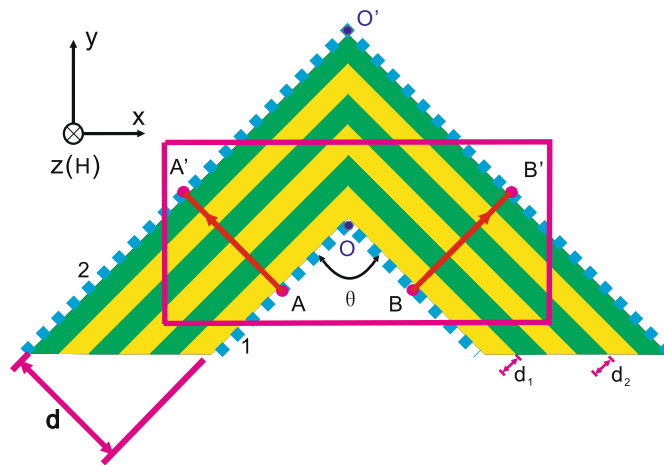


FIGURE 1 Schematics of the VSHLs consisting of a periodic stack of planar Ag and dielectric films with thicknesses d_1 and d_2 , respectively. θ denotes the wedge angle. The blue dotted lines 1 and 2 represent the input and output surfaces of the VSHLs, respectively. Two linear sources (A and B) with a straight distance below subdiffraction limit are symmetrically placed on the input surface of the VSHLs

put. Defining the magnification P of the VSHL as the straight distance of two output images $d_{A'B'}$ divided by that of two linear sources d_{AB} , one gets a magnification factor of about $3.2\lambda/(\lambda/3) \simeq 9.5$. Similarly, in the cases of $\theta = 45^\circ$ (Fig. 2a) and 135° (Fig. 2c), respectively, the calculated straight separations between two output beams on the output surface of the VSHL are about $d_{A'B'} = 12 \times \lambda/3$ and $5.5 \times \lambda/3$, respectively, corresponding to the magnification factors of 12 and 5.5, respectively.

Shrinking the distance between the two sources to $d_{AB} = \lambda/4$ while all the other conditions are the same as that of Fig. 2, we see that the separation between the two output beams on the output surface of the VSHL are about $d_{A'B'} = 16 \times \lambda/4$, $12 \times \lambda/4$, and $7 \times \lambda/4$, much bigger than the diffraction limit with magnification factors of 16, 12, and 7, respectively, as the wedge angle is set at $\theta = 45, 90$, and 135° , respectively. Thereby the premagnification of

the VSHL allows for subsequent processing on subdiffraction limit objects by conventional far-field optics.

From the above results we see that the magnification of the VSHL is dependent on the wedge angle and the distance of two objects. From the geometry, one can get the magnification $P = d_{A'B'}/d_{AB} = 1 + 2d \cos(\theta/2)/d_{AB}$ (θ in the range of 0 to 180°). This means that, in addition to dependence on the wedge angle θ and the distance of two objects d_{AB} , P is also determined by the total thickness d of the VSHL: a thicker VSHL and smaller wedge angle will produce stronger amplification to the object. Most interesting, from the expression, we see that P of the VSHL is inversely proportional to the distance of two objects: the shorter the distance between two objects, the larger the P of the VSHL, which has been demonstrated by FDTD simulation. For example, as d and θ are set at 2λ and 45° while the distance between two lin-

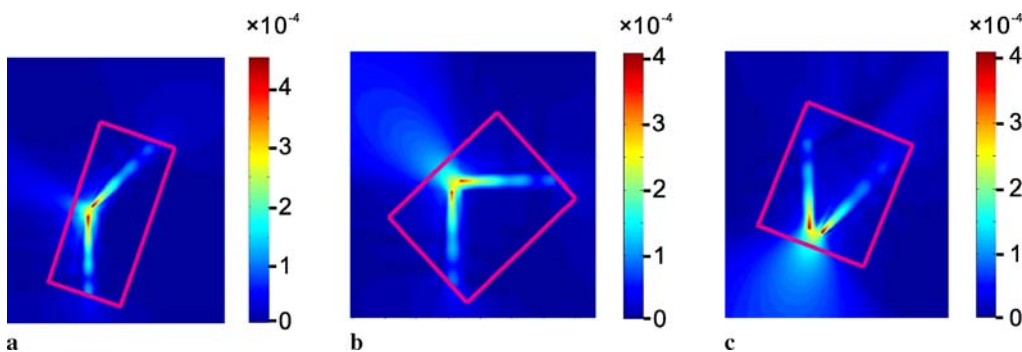


FIGURE 2 Calculated gray distributions of $|H_z|$ in the region bounded by the rectangle shown in Fig. 1, as θ is set at 45° (a), 90° (b), and 135° (c), respectively. The straight distance of the two linear sources is $\lambda/3$, and the total thickness of the VSHL is $d \simeq 2\lambda$, which is constructed with 36 pairs of Ag and dielectric films ($d_1 = d_2 = 10$ nm)

ear objects is $d_{AB} = \lambda/3$ and $\lambda/4$, respectively, we can get the corresponding $P = 12$ and 16 , respectively. Although the magnification of the VSHL is also monotonously enhanced by increasing the total thickness d of the system, the light energy will suffer from stronger attenuation due to longer propagating distance in the metal–dielectric layers. Hence, to balance the magnification and energy loss, one has to select a proper number of the pairs of metal–dielectric layers.

As the objects are illuminated by a plane wave, the scattering light from the region of the two planar layered structures may ultimately limit the imaging performance. To test the effect of the plane wave illumination we simulate the imaging properties of the VSHL as two objects with a space below the diffraction limit are illuminated by a plane wave (Fig. 4a). The objects are two chromium cylinder wires with radius of 20 nm separated by 120 nm. Figure 4b shows the FDTD simulated amplitude distributions of the magnetic field $|H_z|$ as a TM-polarized plane wave is incident into a system with $\theta = 90^\circ$. The relative dielectric constants of chromium at 365 nm wavelength is $\epsilon_m = -8.85 + j8.96$ [4], while other parameters are the same as that of Fig. 2b. From the figure, one can see that in this case no imaging points can be formed at the output surface of the VSHL. To avoid the influence of the central light between the two objects, we cover the inner surface of the VSHL with a 60-nm-thick chromium layer and cut two nanoslits (45 nm wide) with subdiffraction distance (120 nm) on the chromium layer as light scatters (objects) according to [4, 8, 10] (Fig. 4c). The two nanoslits serve as two objects [4, 8, 10], which is similar to the cases where the objects are fluorescence-labeled for bioimaging [24]. Upon light illumination, the scattering light from the two objects will enter into the VSHL and propagate along the normal directions of the layered structure. Figures 4d–f show the amplitude distributions of magnetic field $|H_z|$ in the region bounded by the rectangle denoted in Fig. 4c, as θ is set at 45, 90, and 135°, respectively. From the figures, one can see that the light wave illuminates the whole inner surface of the system but the images of the two objects can clearly be distinguished.

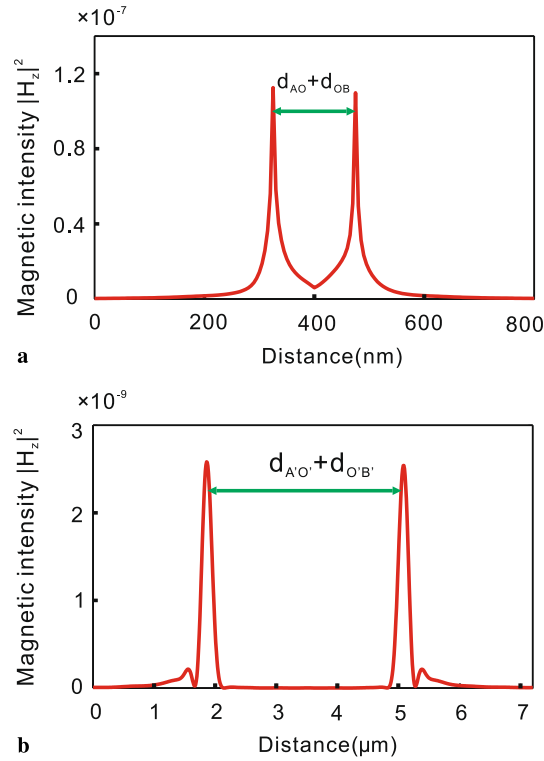


FIGURE 3 Calculated $|H_z|^2$ profiles along the input surface (a) and output surface (b) of the VSHLs. The two linear sources are separated by $\lambda/3$ and the wedge angle θ is 90° , as the case of Fig. 2b

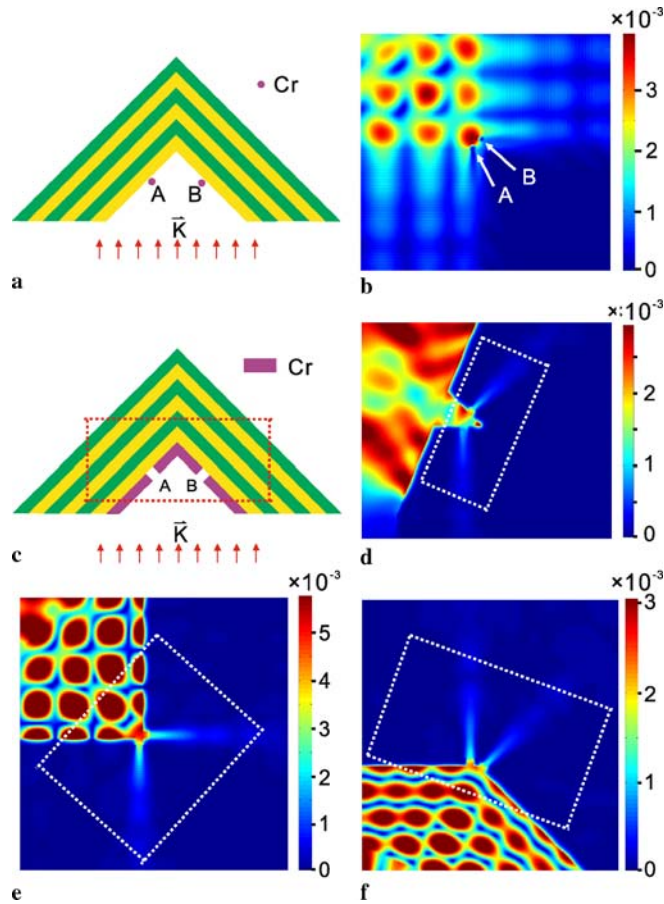


FIGURE 4 (a) Schematic of structures as two Cr nanowires (A, B) are placed near the inner surface of the VSHL. (b) The gray distributions of $|H_z|$ as a TM-polarized plane wave illuminates a VSHL with $\theta = 90^\circ$. (c) Schematic of structures as the inner surface is covered with a chromium layer with two nanoslits (A, B). The simulated gray distributions of $|H_z|$ as θ is set at 45° (d), 90° (e), and 135° (f), respectively, while other parameters are the same as that Fig. 2a–c

3 Mutual interference of two linear sources

Finally, to estimate the mutual interference of two objects with nanoscale separation on the resolving power of the VSHL, we calculate the field distribution of light around the VSHL as only one linear source (A) is placed on the input surface of the system. Figure 5a shown is the $|H_z|$ distribution of light in the region bounded by the rectangle shown in Fig. 1 as the distance $d_{AO} = 80$ nm while other parameters are the same as that of Fig. 2b. One can see that the linear source can form two separated images at the outer boundary surface of the VSHL. Figure 5b shown is the corresponding $|H_z|^2$ profiles of images at points A' and around B'. It can be seen that the optical intensity of the image around point B' is much weaker than that of the image at A'. Introducing optical modulation $M = (I_1 - I_2)/(I_1 + I_2)$ to represent the image contrast, where I_1, I_2 represent the light intensities of the images of points A and B (B and A) at points A' (around B') of the output surface, respectively, then we can get an image contrast of about 0.77 as linear sources A and B are simultaneously involved on the input surface of the VSHL. As the linear source moves towards the corner O of the VSHL, the light intensity of the image of object A around point B' will become stronger and hence M will decrease. For instance, Fig. 5c and d, respectively, show the gray distribution of $|H_z|$ in the rectangular panel of Fig. 1 and $|H_z|^2$ profiles along the output surface at output points A' and around B', as $d_{AO} = 10$ nm while other parameters are the same as that Fig. 5a and b. In this case, we can get an image contrast M of about 0.19. When d_{AO} changes to 15 nm, then the corresponding M is about 0.31 [25], that is to say, as two objects are simultaneously placed at points A and B of the input surface of a VSHL, the two images A' and B' can exactly be distinguished as $d_{AO} = d_{BO} = 15$ nm, which corresponds a straight distance of points A and B of $d_{AB} = 15 \text{ nm} \times \sqrt{2} \approx 21$ nm, much below the diffraction limit.

Figure 6 shows the dependence of the optical modulation M (curves 1–3) and magnification P (curves 4–6) on the distances of two linear sources as θ

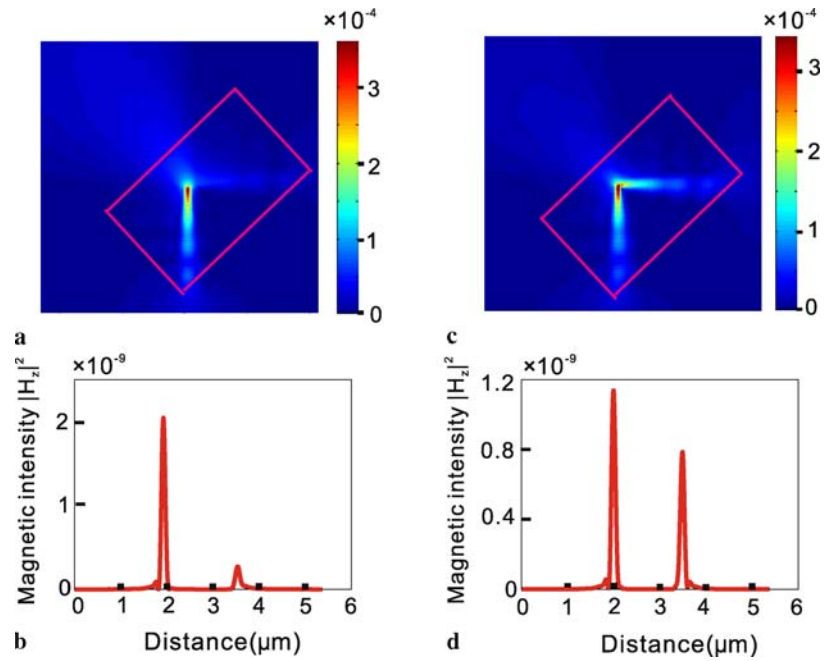


FIGURE 5 Calculated gray distributions of $|H_z|$ in the region bounded by the rectangle shown in Fig. 1 (a and b) and $|H_z|^2$ profiles along the output surface (c and d) as just one linear source is placed at A of the input surface of the VSHLs with $d_{AO} = 80$ and 10 nm, and $\theta = 90^\circ$, respectively

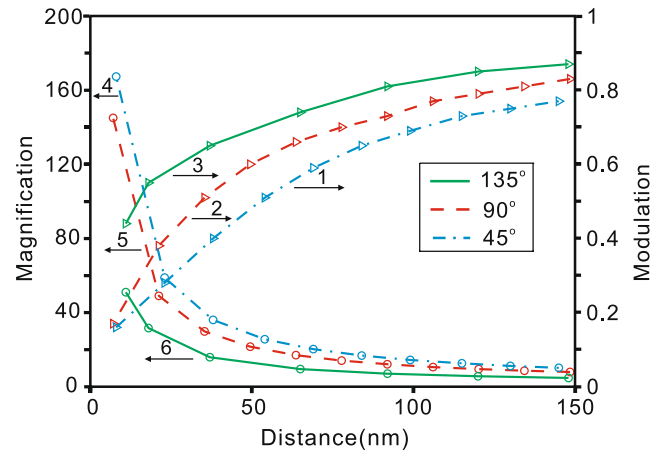


FIGURE 6 Dependence of the optical modulation M (curves 1–3) and magnification P (curves 4–6) on the distances of the two linear sources as θ is set at 45° (dash-dotted line), 90° (dashed line), and 135° (solid line), respectively, while other parameters are the same as that of Fig. 2a–c

is set at 45, 90, and 135° , respectively, while other parameters are the same as that of Fig. 2a–c. It can be seen that P is reduced while M increased with the distance of two scattering sources monotonously. In addition, with the same object distance, M is enhanced but P reduced with the increase of θ . This means that, to balance the magnification and image modulation, one has to properly choose θ .

4 Conclusions

To sum up, VSHLs constructed with v-shaped planar layered

metal–dielectric media are introduced for far-field subdiffraction imaging. Numerical results of the imaging properties from the FDTD simulations demonstrated that two linear sources with a straight distance far below the diffraction limit can be magnified by the systems to the extent that conventional far-field optical microscopy can be further manipulated.

ACKNOWLEDGEMENTS This work is supported by the National Basic Research Program of China (Grant No. 2007CB935304), the National Natural Science Foundation of China (Grant Nos. 60736041, 10774116, 10574101), and the program of NCET (Grant No. 04-0678).

REFERENCES

- 1 E.A. Ash, G. Nicholls, *Nature (London)* **237**, 510 (1972)
- 2 J. Koglin, U.C. Fischer, H. Fuchs, *Phys. Rev. B* **55**, 7977 (1997)
- 3 J.B. Pendry, *Phys. Rev. Lett.* **85**, 3966 (2000)
- 4 N. Fang, H. Lee, C. Sun, X. Zhang, *Science* **308**, 534 (2005)
- 5 T. Taubner, D. Korobkin, Y. Urzhumov, G. Shvets, R. Hillenbrand, *Science* **313**, 1595 (2006)
- 6 Z. Jacob, L.V. Alekseyev, E. Narimanov, *Opt. Express* **14**, 8247 (2006)
- 7 A. Salandrino, N. Engheta, *Phys. Rev. B* **74**, 075 103 (2006)
- 8 Z.W. Liu, H. Lee, Y. Xiong, C. Sun, X. Zhang, *Science* **315**, 1686 (2007)
- 9 Z. Jacob, L.V. Alekseyev, E. Narimanov, *J. Opt. Soc. Am.* **24**, A52 (2007)
- 10 H. Lee, Z.W. Liu, Y. Xiong, C. Sun, X. Zhang, *Opt. Express* **15**, 15 886 (2007)
- 11 E.N. Economou, *Phys. Rev.* **182**, 539 (1969)
- 12 M.J. Bloemer, M. Scalora, *Appl. Phys. Lett.* **72**, 1676 (1998)
- 13 N.N. Lepeshkin, A. Schweinsberg, G. Piredda, R.S. Bennink, R.W. Boyd, *Phys. Rev. Lett.* **93**, 123 902 (2004)
- 14 A. Husakou, J. Herrmann, *Phys. Rev. Lett.* **99**, 127 402 (2007)
- 15 Y.M. Liu, G. Bartal, D.A. Genov, X. Zhang, *Phys. Rev. Lett.* **99**, 153 901 (2007)
- 16 B. Wang, G.P. Wang, *Opt. Lett.* **29**, 1992 (2004)
- 17 X. Fan, G.P. Wang, *Opt. Lett.* **31**, 1322 (2006)
- 18 X. Fan, G.P. Wang, J.C.W. Lee, C.T. Chan, *Phys. Rev. Lett.* **97**, 073 901 (2006)
- 19 S. Feng, J. Elson, *Opt. Express* **14**, 216 (2006)
- 20 D. Schurig, D.R. Smith, *New J. Phys.* **7**, 162 (2005)
- 21 P.A. Belov, Y. Hao, *Phys. Rev. B* **73**, 113 110 (2006)
- 22 J.P. Berenger, *J. Comput. Phys.* **114**, 185 (1994)
- 23 P.B. Johnson, R.W. Christy, *Phys. Rev. B* **6**, 4370 (1972)
- 24 H.E. Daldrup-Link, M. Rudelius, G. Piontek, S. Metz, R. Brauer, G. Debus, C. Corot, J. Schlegel, T.M. Link, C. Peschel, E.J. Rummeny, R.A.J. Oostendorp, *Radiology* **234**, 197 (2005)
- 25 J.R. Meyer-Arendt, *Introduction to Classical and Modern Optics*, 2nd edn., part 2 (Prentice-Hall, Englewood Cliffs, NJ, 1984), pp. 208–211